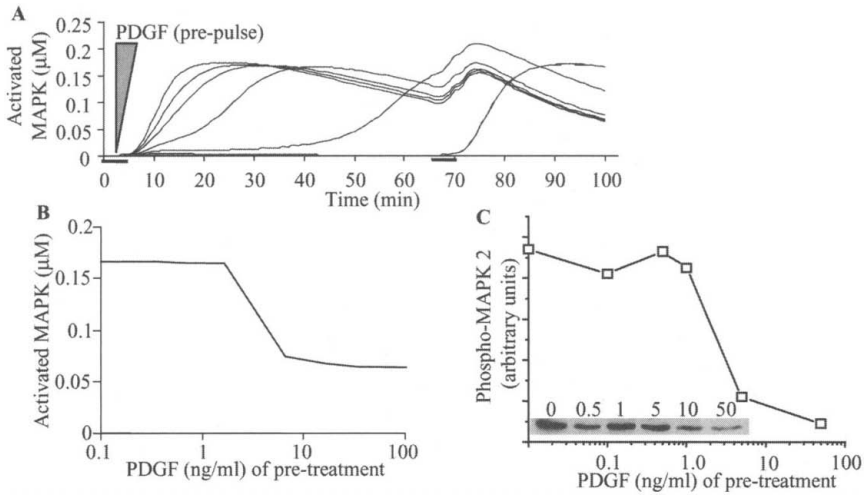

Fig. 5. History-dependent responses of the MAPK system. A varying concentration of PDGF was delivered for 5 min, followed by a wash and reincubation. After 60 min a second stimulation was delivered at 50 ng/ml, which is normally saturating to elicit prolonged MAPK activation. (**A**) Computational traces show range of response time-courses. Initial and second stimulation durations are indicated by horizontal bars. Concentrations of PDGF during the initial stimulation are 20 pM (0.67 ng/ml), 100 pM (3.33 ng/ml), 200 pM (6.67 ng/ml), 500 pM (16.67 ng/ml), 1 nM (33.33 ng/ml), and 100 nM (333.33 ng/ml). (**B**) Computationally derived MAPK activities at the final time point, 100 min after start. (**C**) Effects of pretreatment of NIH-3T3 cells with varying concentrations of PDGF on subsequent stimulation by a saturating concentration. Serum-starved NIH-3T3 cells were stimulated with various concentrations of PDGF as indicated for 5 min, washed, and reincubated for 60 min in serum-free medium. The cells were then restimulated with 50 ng/ml PDGF for 5 min, washed, and incubated for 30 min. Proteins from soluble cell lysate were probed with antibody specific for dual-phosphorylated MAPK (Phospho-MAPK 2).

Current experimental techniques allow us to observe the predicted systems behavior only in a qualitative manner. To determine quantitative accuracy of our models, techniques that quantitatively and selectively measure biochemical reactions within the cell must be developed. Nevertheless, this first glimpse into the systems capabilities of a well-understood and widely used cell signaling system allows us to start unraveling the underlying complexity in nature's design of this controller network.

References and Notes

1. J. D. Jordan, E. M. Landau, R. Iyengar, *Cell* **103**, 193 (2000).
2. D. Bray, *Nature* **376**, 307 (1995).
3. G.Weng, U. S. Bhalla, R. Iyengar, *Science* **284**, 92 (1999).
4. T. J. Hemesath, E. R. Price, C. Takemoto, T. Badalian, D. E. Fisher, *Nature* **391**, 298 (1998).
5. R. J. Davis, *J. Biol. Chem.* **268**, 14553 (1993).
6. S. Nishibe *et al.*, *Science* **250**, 1253 (1990).
7. K. W. Wood, C. Sarnecki, T. M. Roberts, J. Blenis, *Cell* **68**, 1041 (1992).
8. L. L. Lin *et al.*, *Cell* **72**, 269 (1993).
9. R. A. Nemenoff *et al.*, *J. Biol. Chem.* **268**, 1960 (1993).
10. Y. Nishizuka, *Science* **258**, 607 (1992).
11. T. Shinomura, Y. Asaoka, M. Oka, K. Yoshida, Y. Nishizuka, *Proc. Natl. Acad. Sci. U.S.A.* **88**, 5149 (1991).
12. U. S. Bhalla, R. Iyengar, *Science* **283**, 381 (1999).
13. P. Dent, T. Jelinek, D. K. Morrison, M. J. Weber, T. W. Sturgill, *Science* **268**, 1902 (1995).
14. N. Gomez, P. Cohen, *Nature* **353**, 170 (1991).
15. H. Sun, C. H. Charles, L. F. Lau, N. K. Tonks, *Cell* **75**, 487 (1993).
16. J. M. Brondello, J. Pouyssegur, F. R. McKenzie, *Science* **286**, 2514 (1999).
17. U. S. Bhalla, R. Iyengar, *Chaos* **11**, 221 (2001).
18. U. S. Bhalla, in *The Book of GENESIS, Exploring Realistic Neural Models with GEneral NEural SImulation SYstem*, J. M. Bower, D. Beeman, Eds. (Springer-Verlag, Berlin, ed. 2, 1998), chap. 10.
19. Supplementary material is available on *Science* Online.
20. M. S. Shearman, Z. Naor, K. Sekiguchi, A. Kishimoto, Y. Nishizuka, *FEBS Lett.* **243**, 177 (1989).
21. Z. Baharians, A. H. Schonthal, *J. Biol. Chem.* **273**, 19019 (1998).
22. D. R. Alessi *et al.*, *Curr. Biol.* **5**, 283 (1995).
23. K. Dorfman *et al.*, *Oncogene* **13**, 925 (1996).
24. G. Pages *et al.*, *Proc. Natl. Acad. Sci. U.S.A.* **90**, 8319 (1993).
25. R. D. Blitzer *et al.*, *Science* **280**, 1940 (1998).

26. We thank R. Blitzer for critical reading of the manuscript. We also thank the anonymous reviewers for their incisive comments that were most useful in revising this paper. This research was supported by NIH grants GM-54508 and CA-81050 (R.I.) and the Wellcome Trust and NCBS funds (U.S.B.). P.T.R. was supported by an NIH postdoctoral fellowship (grant CA-79134).

Supporting Online Material
www.sciencemag.org/cgi/content/full/297/5583/1018/DC1
Supporting text

10 December 2001; accepted 13 June 2002

Est1p As a Cell Cycle–Regulated Activator of Telomere-Bound Telomerase

Andrew K. P. Taggart, Shu-Chun Teng,* Virginia A. Zakian†

In *Saccharomyces cerevisiae*, the telomerase components Est2p, *TLC1* RNA, Est1p, and Est3p are thought to form a complex that acts late during chromosome replication (S phase) upon recruitment by Cdc13p, a telomeric DNA binding protein. Consistent with this model, we show that Est1p, Est2p, and Cdc13p are telomere-associated at this time. However, Est2p, but not Est1p, also binds telomeres before late S phase. The *cdc13-2* allele has been proposed to be defective in recruitment, yet Est1p and Est2p telomere association persists in *cdc13-2* cells. These findings suggest a model in which Est1p binds telomeres late in S phase and interacts with Cdc13p to convert inactive, telomere-bound Est2p to an active form.

In *S. cerevisiae*, telomeric DNA consists of irregular $C_{1-3}A/TG_{1-3}$ double stranded repeats as well as the G tail, a >30 nucleotide single-stranded overhang of TG_{1-3} DNA that is detectable only in late S phase (*1*, *2*). Telomere length is maintained by telomerase, a specialized reverse transcriptase with an integral RNA template. In yeast, telomerase action requires at least five genes, deficiencies in any or all of which lead to the same *est* (ever shortening telomeres) phenotype, a progressive telomere shortening leading to eventual cell death (*3*). *EST2* and *TLC1* encode the reverse transcriptase and RNA subunit, respectively. Telomerase action in vivo also requires Est1p, Est3p, and Cdc13p, a protein that binds single-stranded TG_{1-3} DNA. A current model for telomerase regulation is that Cdc13p binds G tails in late S phase to recruit a telomerase holoenzyme consisting of Est1p, Est2p, Est3p, and *TLC1* RNA (*4*–

Department of Molecular Biology, Princeton University, Princeton, NJ 08544, USA.

*Present address: Department of Microbiology, College of Medicine, National Taiwan University, Taiwan.
†To whom correspondence should be addressed. E-mail: vzakian@molbio.princeton.edu

6). Consistent with this model, in vivo assays have shown telomerase action is cell cycle limited, occurring in late S phase or G_2-M phase (the period between S and mitosis) but not in G_1 (the prereplicative growth phase of the cell cycle) (7, 8). Because Cdc13p and Est1p interact in biochemical and yeast two-hybrid assays, recruitment is thought to occur via direct binding between these two proteins (5). The requirement for Est1p in telomere maintenance can be bypassed by artificially fusing Cdc13p to Est2p (4). Also, the *est* phenotype of the *cdc13-2* allele, which disrupts an electrostatic bond with Est1p, can be restored by an allele-specific reciprocal mutation (*est1-60*) (6). However, contrary to the expectations of a recruitment model, the *cdc13-2* protein and Est1p interact normally by both biochemical and two-hybrid criteria, suggesting that the functional interaction between Cdc13p and Est1p that is lost in a *cdc13-2* strain occurs at a step other than recruitment (5).

We used chromatin immunoprecipitation (ChIP) to assess the temporal pattern and genetic dependence of Est1p, Est2p, and Cdc13p telomere association in vivo (9). Sheared chromatin was prepared from formaldehyde cross-linked cells and subjected to immunoprecipitation of Est1p, Est2p, Cdc13p, and, as a positive control, Rap1p, the major structural component of telomeric chromatin (10, 11). To allow immunoprecipitation, the chromosomal loci of *EST1*, *EST2*, and *CDC13* were tagged with Myc epitopes (Fig. 1A) (12, 13). Polyclonal antiserum was used to immunoprecipitate Rap1p. We used quantitative multiplex polymerase chain reaction (PCR) to monitor coimmunoprecipitation of three chromosomal loci with each protein: ARO, a control, nontelomeric fragment; ADH, a subtelomeric fragment ~5 kilobase pairs (kbp) from telomere VII-L; and TEL, a unique fragment ~20 base pairs (bp) away from telomere VII-L (Fig. 1B). Enrichment of ADH and TEL over the background amounts in a control Myc antibody precipitate from an untagged strain reflects subtelomeric and telomeric association in vivo, respectively (13). To control for spurious in vitro binding to telomeric DNA in the cell lysate, we also performed immunoprecipitations from mock–cross-linked cells.

In cycling cells, TEL was enriched ~60-fold over background in immunoprecipitates of Rap1p antiserum but not a nonspecific serum (Fig. 1C, lanes 12, 16, and 17, and Fig. 1D). Consistent with previous results that showed Rap1p associates with subtelomeric regions, we also observed enrichment of the ADH sequence (14). Because enrichment of TEL was, for the most part, crosslinker-dependent, these data confirm previous findings that Rap1p binds telomeres in vivo. Similarly, specific, crosslinker-dependent TEL enrichment for Cdc13p that was dependent on its DNA binding domain (~30-fold; lanes 9, 15, and 18 to 20 of Fig. 1, C and D) confirms previous findings that Cdc13p binds telomeres in vivo (12, 15). Lastly, we observed specific, crosslinker-dependent TEL enrichment for Est1p and Est2p (~3.5-fold and ~16-fold; lanes 7, 8, 13, and 14 of Fig. 1, C and D). Therefore, each of the telomerase pathway components, Cdc13p, Est1p, and Est2p, associates specifically with telomeres in vivo.

We examined Cdc13p telomere binding through the cell cycle (9). The tagged Cdc13p strain was synchronized in G_1 phase with α factor and released into the cell cycle, and samples were assayed by ChIP. Control untagged cells were synchronized simultaneously to determine background at each time point. Fluorescence-activated cell sorter (FACS) analysis of samples showed that progress through the cell cycle was indistinguishable for Myc-tagged and untagged cells; it also showed that S phase had begun at the 30-min time point, was almost complete at 45 min, and was finished at 60 min (fig. S1). The experiment was ended at 105 min, before mitotic cytokinesis. Western blot analysis of whole-cell extracts revealed that the level of Cdc13p increased ~twofold over the course of the experiment (Fig. 2A), consistent with the doubling of mass as cells progressed through the cell cycle and formed buds. Cdc13p was telomere-associated in G_1 phase, and this association persisted through the beginning of S phase (Fig. 2B, lanes 5 to 10; additional G_1 phase data for Cdc13p, Est2p, and Est1p are in fig. S2). A large increase in association was observed in late S phase, peaking at 60 min (~70-fold; lanes 11 to 14 of Fig. 2B). Given that G tails form in late S phase and multiple copies of Cdc13p can bind the same DNA molecule, this increase in association is most consistent with Cdc13p

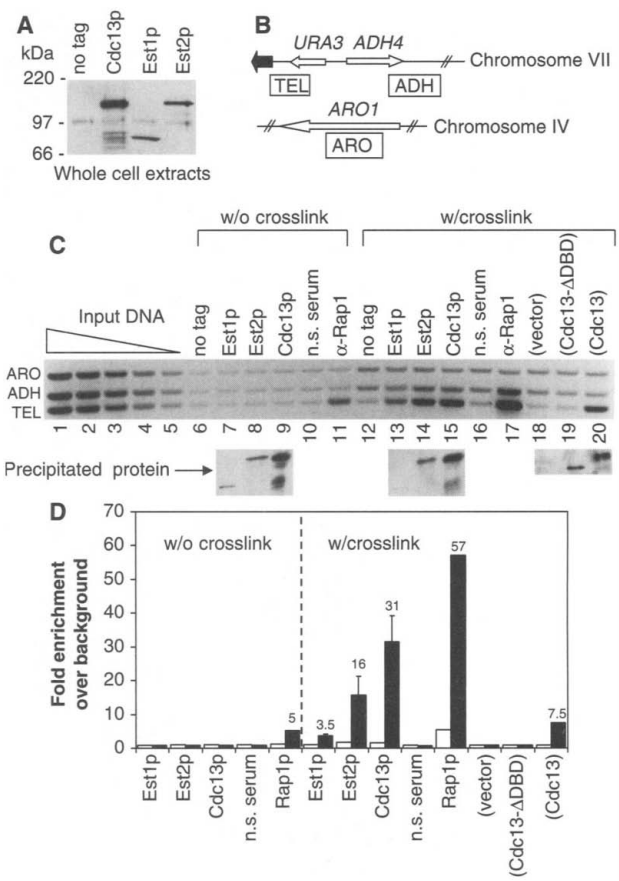

Fig. 1. Est1p, Est2p, and Cdc13p are telomere-associated in vivo. ChIP was performed in either wild-type (not tagged) or strains containing Myc-tagged Est1p, Est2p, or Cdc13p (13). Soluble chromatin from formaldehyde (w/crosslink) or mock treated (w/o crosslink) cells was immunoprecipitated with antibody to Myc, nonspecific serum, or polyclonal Rap1p antiserum. (**A**) Western blot probed with antibody to Myc of whole-cell extracts from the no tag and Myc epitope–tagged strains. Identical cell equivalents were loaded in each lane. (**B**) Schematic of TEL, ADH, and ARO chromosomal loci monitored by ChIP; solid black arrow represents telomere VII-L. Open arrows represent *URA3*, *ADH4*, and *ARO1* open reading frames and their directions of transcription. (**C**) Multiplex PCR results of a representative ChIP experiment. Twofold serial dilutions of the input DNA delineate the linear range of PCR (lanes 1 to 5); the remaining results are from precipitated DNA. Immunoprecipitation was performed on the strains indicated using antibodies to Myc (lanes 6 to 9, 12 to 15, and 18 to 20), nonspecific serum (lanes 10 and 16), or antiserum to Rap1p (lanes 11 and 17). Parentheses refer to either empty vector or plasmids expressing Myc-tagged Cdc13p or a derivative lacking the DNA binding domain (Cdc13-ΔDBD). These plasmids were introduced into a wild-type background, so competition with endogenous untagged Cdc13p lowered TEL enrichment. A fraction of immunoprecipitated material was subjected to a Western blot using antibody to Myc to allow comparison of protein yields. (**D**) Data from (C) are expressed as x-fold enrichment of ADH (open bar) and TEL (solid bar) over background as described in (13). Samples showing substantial telomere association have fold enrichment written (numeral) above the bars. Open bars, ADH; solid bars, TEL. Error bars represent the standard error from multiple independent experiments. Results without error bars were observed in ≥two experiments.

multimerization on G tails (*16*). Later in the cell cycle, association decreased to a lower but still significant level (lanes 15 to 20 of Fig. 2B; this level was consistent with that seen in nocodazole-arrested cells, fig. S2).

Cell cycle analysis for Est2p showed no changes in protein levels other than the gradual twofold increase caused by bud growth (Fig. 2A). Despite observations that telomerase does not act at this time, strong Est2p telomere association was observed in G_1 phase cells (Fig. 2B, lanes 5 to 8; fig. S2). This high level of association was followed by a reduction in signal in early S phase (30 min), which was in turn followed by another strong peak of association in late S phase (45 min; lanes 9 to 12 of Fig. 2B). Lower levels of Est2p association were observed later in the cell cycle and also in nocodazole arrested cells (Fig. 2B, lanes 15 to 20; fig. S2). This pattern was reproducible in five of five independent experiments and was also observed for telomere VI-R (fig. S3) (*17*). Variations in association over time were not due to changes in Est2p immunoprecipitation efficiency (Fig. 2A). A second synchrony technique, in which cells were arrested in telophase using the temperature sensitive *cdc15-2* allele and were released into the cell cycle, confirmed this pattern. After low Est2p telomere association in arrested M phase cells, two peaks of association were again observed, one in G_1 phase and the other in late S (*17*).

Cell cycle analysis of Est1p revealed relatively low levels of protein in G_1 phase cells, followed by a marked ~two- to threefold increase once S phase was underway (30 min; Fig. 2A). After this point, protein levels continued to increase gradually, concomitant with the general increase in cell mass. The increase in Est1p levels in early S phase was in good agreement with previous work that showed transcription of *EST1* is induced late in G_1 (*18*). Thus, Est1p abundance is cell cycle regulated. We observed no Est1p telomere binding in G_1 and early S phase (Fig. 2B, lanes 5 to 10; fig. S2). However, a peak of Est1p telomere binding began in late S phase at 45 min and peaked at 60 min (Fig. 2B, lanes 11 to 14). Est1p binding at 45 min was concurrent with the late S phase peaks of Cdc13p and Est2p association. Thus, all three proteins, Est1p, Est2p, and Cdc13p, were telomere-associated in late S phase, a time when telomerase action has been observed in vivo.

The telomerase-null phenotype of the *cdc13-2* allele has been interpreted as eliminating telomerase recruitment due to disrupted interaction between Cdc13p and Est1p (*6*, *19*). This model predicts that neither Est1p nor Est2p will be telomere-associated in a *cdc13-2* background. However, telomere association of both Est1p and Est2p was normal in cycling *cdc13-2* cells (Fig. 3B, lanes 6, 8, 17, and 19; fig. S4). As a control, we also monitored binding in a *tlc1*Δ background. The steady state level of Est2p in cycling *tlc1*Δ cells was reduced ~twofold, but was not reduced in *cdc13-2* cells (Fig. 3A). This effect was specific; a *TLC1* deletion affected neither Cdc13p nor Est1p levels (Fig. 3A). Thus, *TLC1* RNA is required for full stability of Est2p in vivo. In addition, *TLC1* was required for Est2p but not Cdc13p telomere association (Fig. 3B, lanes 5-7 and 9-10). Est1p telomere association was also substantially decreased in the *tlc1*Δ strain (Fig. 3B, lanes 16 to 18; fig. S4).

We examined Est2p association throughout the cell cycle in synchronized *cdc13-2* cells. Est2p telomere association was similar to wild-type at all time points tested except in late S phase (45 min), when the peak of

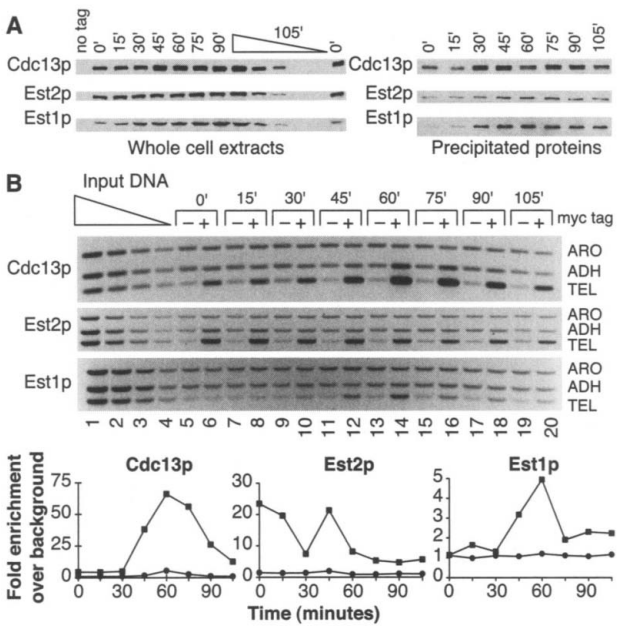

Fig. 2. Cell cycle regulation of Cdc13p, Est2p, and Est1p telomere association. Untagged and Myc-tagged strains were arrested in late G_1 with α factor (0 min), and a portion of each was removed for ChIP using antibodies to Myc. α factor was then removed, allowing synchronous progression through the cell cycle. Samples were taken every 15 min. Early S phase occurred at 30 min; late S, at 45 and 60 min (fig. S2). (**A**) Using antibody to Myc, Western blot of Myc-tagged proteins in whole-cell extracts as well as immunoprecipitated protein over time. Identical cell equivalents are loaded. To allow quantitation of protein levels, twofold serial dilutions of the 105-min whole-cell extract are shown. (**B**) Representative cell cycle ChIP time courses. Multiplex PCR results from the no tag and tagged samples from each time point are shown side by side. The Myc tag–dependent fold enrichment of ADH (solid circle) and TEL (solid square) over background was determined independently for each time point (*13*). In each case, results were observed in ≥two experiments.

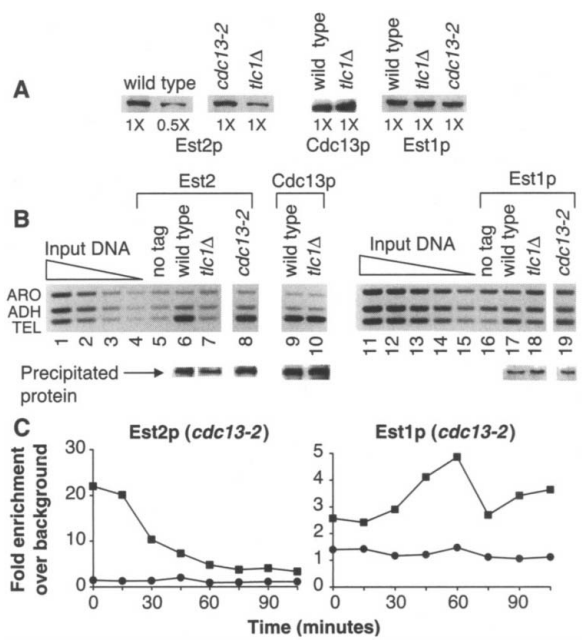

Fig. 3. Est2p, Cdc13p, and Est1p telomere association in *tlc1*Δ and *cdc13-2* backgrounds. Cycling Myc-tagged Est2, Cdc13p, or Est1p cells with wild-type, *tlc1*Δ, or *cdc13-2* backgrounds were subjected to ChIP. (**A**) Using antibody to Myc, Western blots of whole-cell extracts from cycling Myc-tagged Est2p, Est2p *cdc13-2*, Est2p *tlc1*Δ, Cdc13p, Cdc13p *tlc1*Δ, Est1p, Est1p *tlc1*Δ, and Est1p *cdc13-2* strains. Identical (1×) cell equivalents were loaded except for wild-type Est2p, where 1× and 0.5× cell equivalents are shown. (**B**) Multiplex PCR results (for quantitation of these data, see fig. S4). Relative yields of precipitated proteins are shown. (**C**) Cell cycle ChIP time courses on Myc-tagged Est2p and Est1p *cdc13-2* cells. Experiments were performed as in Fig. 2. FACS profiles and protein levels at each time point were identical to wild-type (*17*). Representative fold TEL (solid square) and ADH enrichments (solid circle) above background at each time point are shown. In each case, results were observed in ≥two experiments.

association observed in wild-type cells was missing in the mutant (Fig. 3C, fig. S5). The missing late S phase peak was not due to an absence of telomere-bound Cdc13p, as we observed no difference in telomere binding between *cdc13-2* protein and wild type Cdc13p (*17*). For Est1p, cell cycle ChIP showed that, if anything, telomere binding was slightly enhanced at most time points in *cdc13-2* cells (Fig. 3C, fig. S5). The *cdc13-2* allele is deficient in interaction with Stn1p (*20*). It is possible that the increase in Est1p telomere association in *cdc13-2* cells reflects increased telomere accessibility due to a lack of steric hindrance from Stn1p. Regardless, from these data we conclude that Est1p is fully able to associate with telomeres in a *cdc13-2* background.

Telomerase action is not observed in G_1 phase cells, yet we observed strong *TLC1*-dependent telomere association of Est2p, the catalytic subunit, at that time point (Figs. 2 and 3, fig. S2). Access of the Est2p-*TLC1* RNA complex to chromosome ends is, therefore, not sufficient for telomerase action in vivo. The Est2p signal was decreased, but not eliminated, in early S phase, reflecting either dissociation of Est2p from a subset of telomeres or decreased cross-linking efficiency, possibly through a change in conformation or in neighboring components of telomeric chromatin. We observed a second peak of Est2p telomere association in late S phase (Fig. 2B). The fact that this peak did not occur in the telomerase-defective *cdc13-2* background suggests that it reflects an essential process for telomerase action in vivo (Fig. 3C, fig. S5). Our findings suggest that two key events are concurrent with the late S phase Est2p peak: multimerization of Cdc13p on the G tail and Est1p binding. We propose that Est1p is a cell cycle regulated (Fig. 2A) activator of telomerase that binds to an inactive, telomere-bound Est2p-*TLC1* RNA complex in late S phase and then interacts with one or more Cdc13p molecules arrayed on the G tail. This interaction changes the state of bound Est2p, either through binding of additional Est2p (e.g., dimerization) (*21*) or a conformational change that enhances cross-linking; this is manifested as the late S phase peak of Est2p telomere association and results in activation of telomerase for synthesis. The *cdc13-2* mutation disrupts a functional interaction with Est1p (*6*). Because Est1p telomere association is robust in *cdc13-2* cells (Fig., 3, B and C), this functional interaction must be separable from and downstream of Est1p telomere binding. We propose the telomerase deficiency of the *cdc13-2* allele reflects failure to interact properly with telomere bound Est1p to promote activation, resulting in persistence of inactive Est2p at the telomere and concurrent loss of the late S phase peak. We detected decreased but still considerable Est2p telomere association after S phase (Fig. 2B; fig. S2), suggesting that at least a subset of Est2p remains bound to telomeres for the remainder of the cell cycle, perhaps as a protective cap (*21*). Because the G_1 peak of association followed low association in M phase (*17*), Est2p appears to load onto telomeres again at the beginning of the next cell cycle.

References and Notes

1. V. A. Zakian, *Science* **270**, 1601 (1995).
2. R. J. Wellinger, K. Ethier, P. Labrecque, V. A. Zakian, *Cell* **85**, 423 (1996).
3. C. I. Nugent, V. Lundblad, *Genes Dev.* **12**, 1073 (1998).
4. S. K. Evans, V. Lundblad, *Science* **286**, 117 (1999).
5. H. Qi, V. A. Zakian, *Genes Dev.* **14**, 1777 (2000).
6. E. Pennock, K. Buckley, V. Lundblad, *Cell* **104**, 387 (2001).
7. S. J. Diede, D. E. Gottschling, *Cell* **99**, 723 (1999).
8. S. Marcand, V. Brevet, C. Mann, E. Gilson, *Curr. Biol.* **10**, 487 (2000).
9. O. M. Aparicio, D. M. Weinstein, S. P. Bell, *Cell* **91**, 59 (1997).
10. M. N. Conrad, J. H. Wright, A. J. Wolf, V. A. Zakian, *Cell* **63**, 739 (1990).
11. J. H. Wright, D. E. Gottschling, V. A. Zakian, *Genes Dev.* **6**, 197 (1992).
12. Y. Tsukamoto, A. K. P. Taggart, V. A. Zakian, *Curr. Biol.* **11**, 1328 (2001).
13. Materials and Methods are available as supporting online material on *Science* Online.
14. S. Strahl-Bolsinger, A. Hecht, K. Luo, M. Grunstein, *Genes Dev.* **11**, 83 (1997).
15. B. D. Bourns, M. K. Alexander, A. M. Smith, V. A. Zakian, *Mol. Cell. Biol.* **18**, 5600 (1998).
16. T. R. Hughes, R. G. Weilbaecher, M. Walterscheid, V. Lundblad, *Proc. Natl. Acad. Sci. U.S.A.* **97**, 6457 (2000).
17. A. K. P. Taggart, V. A. Zakian, unpublished data.
18. P. T. Spellman *et al.*, *Mol. Biol. Cell* **9**, 3273 (1998).
19. C. I. Nugent, T. R. Hughes, N. F. Lue, V. Lundblad, *Science* **274**, 249 (1996).
20. A. Chandra, T. R. Hughes, C. I. Nugent, V. Lundblad, *Genes Dev.* **15**, 404 (2001).
21. J. Prescott, E. Blackburn, *Genes Dev.* **11**, 2790 (1997).

22. We thank M. K. Alexander, H. Qi, W. H. Tham, S. Schnakenberg, and L.Vega for critical reading of the manuscript. This work was supported by the National Institutes of Health grant GM43265 (to V.A.Z.). A.K.P.T was supported in part by a postdoctoral fellowship from the Susan G. Komen Breast Cancer Foundation and also NIH grant T32 CA09528-16.

Supporting Online Material
www.sciencemag.org/cgi/content/full/297/5583/1023/DC1
Materials and Methods
Figs. S1 to S5
Table S1

11 June 2002; accepted 3 July 2002

Orc6 Involved in DNA Replication, Chromosome Segregation, and Cytokinesis

Supriya G. Prasanth, Kannanganattu V. Prasanth, Bruce Stillman*

Origin recognition complex (ORC) proteins serve as a landing pad for the assembly of a multiprotein prereplicative complex, which is required to initiate DNA replication. During mitosis, the smallest subunit of human ORC, Orc6, localizes to kinetochores and to a reticular-like structure around the cell periphery. As chromosomes segregate during anaphase, the reticular structures align along the plane of cell division and some Orc6 localizes to the midbody before cells separate. Silencing of Orc6 expression by small interfering RNA (siRNA) resulted in cells with multipolar spindles, aberrant mitosis, formation of multinucleated cells, and decreased DNA replication. Prolonged periods of Orc6 depletion caused a decrease in cell proliferation and increased cell death. These results implicate Orc6 as an essential gene that coordinates chromosome replication and segregation with cytokinesis.

The initiation of DNA replication in eukaryotic cells is a highly regulated process that leads to the duplication of the genetic information for the next cell generation. Duplication of chromosomes in S phase is followed by segregation of the resultant sister chromatids during mitosis (*1*). Initiation of DNA replication is mediated by a conserved set of proteins, including ORC, which is bound to origins of DNA replication and is highly conserved (*2–4*). In human cells, ORC consists of six subunits. In *Drosophila* embryos, Orc6 forms a complex with other ORC subunits, but there is a major fraction of Orc6 that is not part of the ORC complex, a function for which is hitherto unknown (*5, 6*). Although ORC acts as a DNA replication initiator protein, it is known to function in other cellular processes such as transcriptional gene silencing and heterochromatin formation (*2*). To function in DNA replication, ORC proteins need to be recruited to chromatin, but their fate during mitosis has not been clearly established.

We used immunofluorescence to investigate the cell cycle localization of Orc6 protein in human cells. The polyclonal antibody to Orc6 (anti-Orc6) (*7*) was highly specific (fig. S1). Orc6 was localized in the nucleus

Cold Spring Harbor Laboratory, 1 Bungtown Road, Cold Spring Harbor, NY 11724, USA.

*To whom correspondence should be addressed. E-mail: stillman@cshl.org